

A Photochemically Generated Selenyl Free Radical Observed by High Energy Resolution Fluorescence Detected X-ray Absorption Spectroscopy

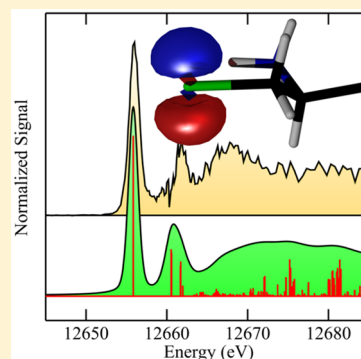
Susan Nehzati,[†] Natalia V. Dolgova,[†] Dimosthenis Sokaras,[‡] Thomas Kroll,[‡] Julien J. H. Cotelesage,[†] Ingrid J. Pickering,^{†,§,Ⓜ} and Graham N. George^{*,†,§,Ⓜ}

[†]Molecular and Environmental Sciences Group, Department of Geological Sciences, University of Saskatchewan, Saskatoon, Saskatchewan S7N 5E2, Canada

[‡]Stanford Synchrotron Radiation Lightsource, SLAC National Accelerator Laboratory, Stanford University, Menlo Park, California 94025, United States

[§]Department of Chemistry, University of Saskatchewan, Saskatoon, Saskatchewan S7N 5C9, Canada

ABSTRACT: Selenium-based selenyl free radicals are chemical entities that may be involved in a range of biochemical processes. We report the first X-ray spectroscopic observation of a selenyl radical species generated photochemically by X-ray irradiation of low-temperature solutions of L-selenocysteine. We have employed high energy resolution fluorescence detected X-ray absorption spectroscopy (HERFD-XAS) and electron paramagnetic resonance (EPR) spectroscopy, coupled with density functional theory calculations, to characterize and understand the species. The HERFD-XAS spectrum of the selenyl radical is distinguished by a uniquely low-energy transition with a peak energy at 12 659.0 eV, which corresponds to a $1s \rightarrow 4p$ transition to the singly occupied molecular orbital of the free radical. The EPR spectrum shows the broad features and highly anisotropic g -values that are expected for a selenium free radical species. The availability of spectroscopic probes for selenyl radicals may assist in understanding why life chooses selenium over sulfur in selected biochemical processes.



1. INTRODUCTION

The chemistries of sulfur and selenium have many similarities.¹ Both elements are important in biology, with sulfur being one of the six elements that are central to all life, and selenium playing important roles in redox homeostasis. Selenium is distinguished among the elements of life as having the lowest crustal abundance,² and is incorporated into biological molecules at tremendous metabolic cost.³ It is further distinguished as the element with the smallest differential between a dietary level that is appropriate for good human health, and a toxic excess; a phenomenon that has caused Jukes to dub selenium as an “essential poison”.⁴ The physiologically important selenolate ($R-Se^-$), found as the L-selenocysteine form of the amino acid, is possibly the strongest nucleophile to be found in living systems, but many open questions remain as to why it is so biologically important.

Thiyl radicals ($R-S\cdot$) are well-known in both chemistry and biology; they have been exploited in synthetic organic chemistry,⁵ while in biology, they have been implicated in a range of biological processes,^{6–8} such as the catalytic mechanism of ribonucleotide reductases.⁹ In contrast to thiyl radicals, the analogous selenium-based selenyl radicals ($R-Se\cdot$),¹⁰ sometimes called selanyl radicals, have been implicated only rarely.¹¹ Differences in reactivity between thiyl and selenyl radicals have been used to explain why nature uses selenium in preference to sulfur in some biological molecules.¹² Thiyl

radicals are notoriously difficult to observe directly,^{5,13–15} and most frequently indirect methods such as spin-trapping have been used.⁸ To our knowledge, there are currently no reports of direct observations of selenyl radicals.

Photochemical modification of elements of interest in X-ray absorption spectroscopy (XAS) experiments is a well-established problem¹⁶ against which various experimental strategies have been developed;¹⁷ we recently exploited this photochemistry to enable a study of thiyl radicals using sulfur K-edge XAS.¹³ We report herein the first direct X-ray spectroscopic observation of photochemically generated selenyl radicals in cryogenic aqueous solutions of the biologically relevant selenol, selenocysteine.

2. MATERIALS AND METHODS

2.1. Sample Preparation. Reagents were purchased from Sigma-Aldrich (Oakville, ON) and were of the highest quality available. Aqueous solutions of L-selenocysteine (1 mM final concentration) were prepared by reduction of the diselenide L-selenocysteine with sodium borohydride as described by Pickering et al.,¹⁸ loaded into 2 mm thick polyacetal cuvettes closed with a mylar tape window, and then frozen by immersion into a partly frozen isopentane slurry with a temperature of approximately 120 K. Samples were transported and stored at liquid nitrogen temperatures until data acquisition.

Received: June 1, 2018

Published: August 22, 2018

2.2. High Energy Resolution Fluorescence Detected X-ray Absorption Spectroscopy. High energy resolution fluorescence detected (HERFD) XAS measurements were carried out at the Stanford Synchrotron Radiation Lightsource (SSRL) using beamline 6-2 with the SPEAR3 storage ring containing 500 mA at 3.0 GeV. A Si(311) double crystal monochromator having an energy resolution at the Se K-edge of ~ 0.4 eV was used for the incident beam, together with a 6-element array of Si(844) crystal analyzers to record the Se $K\alpha_1$ emission line,¹⁹ with an overall energy resolution of 0.95 eV measured using scans of the elastic scattering. The incident and transmitted X-rays were monitored using gas ionization chambers filled with helium and nitrogen, respectively. An in-hutch photon shutter was employed to prevent exposure of the sample when data were not being actively recorded to ensure accurate exposure times, and aluminum filters upstream of the incident ion chamber were used to adjust X-ray exposures. Samples were maintained at a temperature of 10 K using a helium flow cryostat (Oxford instruments, Abingdon, U.K.) and were inclined at an angle of 45° to the incident X-ray beam to facilitate measurement of X-ray fluorescence, giving an incident X-ray path length of 2.8 mm. Energy calibration of the monochromator was relative to the lowest-energy inflection of a gray hexagonal selenium foil, which was assumed to be 12 658.0 eV. Data reduction and analysis was carried out as previously described²⁰ using the EXAFSPAK suite of computer programs (<http://ssrl.slac.stanford.edu/exafspak.html>).

2.3. Electron Paramagnetic Resonance (EPR) Spectroscopy. EPR spectroscopy was carried out using a JEOL REIX X-band instrument (JEOL, Tokyo, Japan) located adjacent to the beamline at SSRL, and employing a sample temperature of 80 K. Irradiated samples were transported under liquid nitrogen directly from the beamline to the EPR spectrometer, and their EPR spectra were recorded immediately.

2.4. Density Functional Theory (DFT) Calculations. DFT geometry optimizations were carried out using DMol³ and Biovia Materials Studio Version 2017 R2^{21,22} using the Perdew–Burke–Ernzerhof functional both for the potential during the self-consistent field procedure, and for the energy.^{23,24} DMol³ double numerical basis sets included polarization functions for all atoms with all-electron relativistic core treatments. Environmental effects were modeled using the Conductor-like Screening Model (COSMO)²⁵ in DMol³, with a dielectric value representing water ($\epsilon = 78.54$).

DFT simulations of near-edge spectra were calculated using the StoBe-deMon code²⁶ employing the half-core-hole approximation for the core-hole, incorporating relaxation of selected excited states at the absorption edge, and employing the coordinates from DMol³ geometry optimizations. StoBe-deMon calculations employed the nonlocal exchange function of Perdew and Wang²⁷ and the Perdew correlation functional approximation.^{28,29} The (6311/311/1) basis set was used for carbon and (311/1) for hydrogen. For selenium, the (63321/5321/41) basis set was employed. Interpolation of the exchange-correlation potential employed the auxiliary basis sets (5,5;5,5) for selenium, (5,2;5,2) for carbon, nitrogen and oxygen, and (3,1;3,1) for hydrogen. Computed spectra for open-shell free radical species were averages of α and β symmetry; convolution with pseudo-Voigt line shape functions was conducted as previously described.³⁰

3. RESULTS AND DISCUSSION

3.1. X-ray Absorption Spectroscopy. In the present work, we employ HERFD-XAS,³¹ which uses a high-resolution X-ray spectrometer to measure the X-ray fluorescence with considerably better resolution than the natural line width. In conventional K-edge XAS, the short lifetime of the 1s core-hole causes a substantial broadening of the spectra, with a consequent loss of detail and chemical sensitivity. Our Se K-edge HERFD-XAS employs the Se $K\alpha_1$ fluorescence line, and effectively observes just a subset of the $2p_{3/2} \rightarrow 1s$ transitions that give rise to the Se $K\alpha_1$. This eliminates most of the

lifetime broadening from the 1s core-hole, enormously enhancing the spectral resolution. The residual observed broadening of the HERFD-XAS spectra is dominated by core-hole lifetime broadening of the $2p_{3/2}$ hole that is created with the formation of the $K\alpha_1$ fluorescent photon,³² convoluted with broadening functions arising from the energy resolution of the emission spectrometer and to a small extent from the beamline. The HERFD-XAS method requires a near 90° analyzer Bragg angle θ_B [Si(844) has $\theta_B \approx 85.2^\circ$ at the Se $K\alpha_1$ energy of 11 224 eV] and the use of a tightly focused incident X-ray beam (SSRL beamline 6-2 has a beam size of 0.3×0.1 mm² at 12.6 keV). During experiments designed to characterize the capabilities of HERFD-XAS for biological studies, we observed striking photochemical changes in solutions of L-selenocysteine at a pH of 2.0, chosen to ensure protonation of the selenol which has a pK_a of 5.47;³³ at this pH, both the carboxylic acid and the amino group of the amino acid also will be in their protonated states. For convenience in discussion of the chemistry around selenium, we abbreviate L-selenocysteine as Cys–SeH, where, in this case, Cys– denotes the fragment $\text{HO}_2\text{C}(\text{H}_3\text{N}^+)\text{CHCH}_2-$.

Figure 1 shows the progressive changes in the HERFD-XAS spectra of a solution of Cys–SeH with increasing X-ray

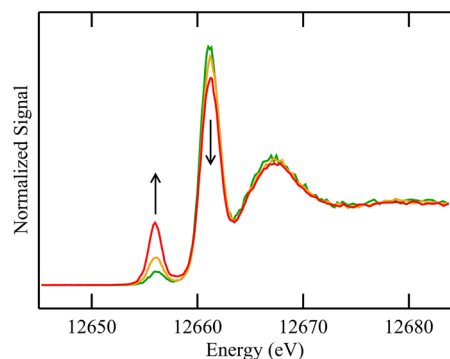


Figure 1. Changes with increasing X-ray dose in the Se K-edge HERFD-XAS spectra of a 1 mM solution of L-selenocysteine at pH 2.0, corresponding to calculated absorbed radiation doses of 0.5 MGy (green line), 1.0 MGy (yellow line), and 2.9 MGy (red line). The arrows indicate the direction of the change in the spectra with increasing dose.

exposure, with three individual 2 min sweeps superimposed. A low-energy peak at approximately 12 656.0 eV is observed to appear and to accumulate in intensity with increased X-ray exposure. The difference spectrum, which should correspond to approximately 100% of the photochemical product, is shown in Figure 2 together with the spectrum of pure starting Cys–SeH, also obtained by difference. The 12 656.0 eV peak energy of this product species is unusually low for a selenium K-edge spectrum, with the lowest-energy features for inorganic selenides (Se^{2-}) typically falling around 12 659 eV. The spectrum bears a striking resemblance to the sulfur K-edge conventional XAS spectra recently reported by us for thiyl radicals,¹³ allowing for the approximately 10 189 eV difference between the sulfur and selenium K-edge threshold energies. The species with the 12 659.0 eV peak does not form upon irradiation of the deprotonated L-selenocysteinate Cys–Se⁻ (not illustrated) prepared similarly but at a higher pH, and instead a different species with a peak energy ~ 1 eV higher is produced at much lower rates. Because of these considerations,

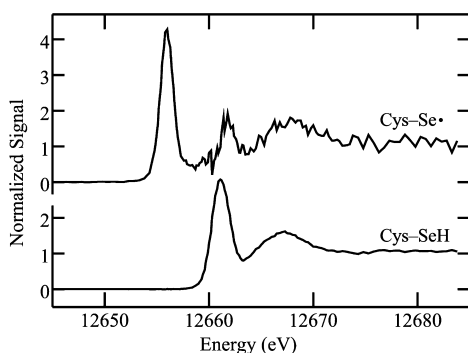
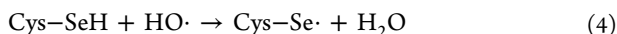
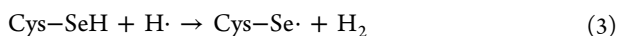
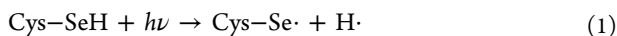


Figure 2. Difference selenium K-edge HERFD-XAS spectra corresponding to 100% reactant Cys–SeH (R–SeH), and 100% photochemical product Cys–Se•. The difference spectrum for Cys–SeH was generated by subtracting a fraction of the high-dose spectrum from that of the lowest dose to eliminate the low-energy feature. Similarly, the spectrum of Cys–Se• was obtained by subtracting small increments of the low dose from the high-dose spectrum, until just before the appearance of negative features corresponding to the peak signal intensity of Cys–SeH.

we assign the observed 12 659.0 eV low-energy feature to the selenyl radical Cys–Se•. We hypothesize that the photochemical reaction proceeds either by a direct photochemical process (eq 1) or through chemistry involving the photolysis products of water (eqs 2–4):



SSRL beamline 6-2 has a very high flux density of 1.3×10^{14} photons $\text{s}^{-1} \text{mm}^{-2}$; at similar high flux densities, evolution of bubbles of H_2 from X-ray irradiation of room-temperature aqueous solutions has previously been reported, probably arising through combination of two $\text{H}\cdot$ radicals.³⁴ The capability of direct generation of alkylselenyl radicals by breakage of Se–H bonds can be estimated from the Se–H bond dissociation energies which, at about 330 kJ mol^{-1} (or 3.4 eV),³⁵ are substantially less than the X-ray energy employed in our experiments. The hydrogen radicals generated in eqs 1 and 2 are likely to engage in further chemistry; in our system, the large excess of water will likely form hydrated electrons, which can reduce redox active species, and can be clearly seen as a beam mark on the irradiated sample from color centers arising from hydrated electrons (eq 5) trapped in the ice matrix.¹⁷



3.2. Ground State Density Functional Theory Calculations. Figure 3 shows the results of energy minimized geometry optimized DFT of Cys–Se•, superimposed with the spin density isosurface, together with a schematic structure of the species, labeled with the computed atomic Mulliken spin populations. The spin densities of the free radical species are seen to be highly localized on the selenium, with the singly occupied molecular orbital being an almost pure Se 4p orbital. Abstraction of a proton from the amino group could potentially yield tautomeric structures with –SeH and a nitrogen-centered free radical. DFT computation of this

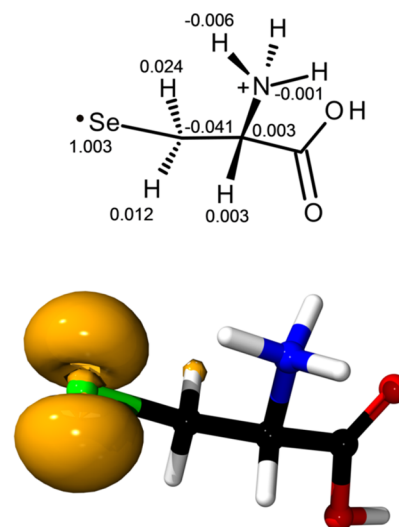


Figure 3. DFT computed ground state spin density of Cys–Se• showing the schematic structure (top) together with the energy minimized geometry optimized structure and the spin density isosurface corresponding to 0.05 spins per a.u.³ (bottom). Computed atomic Mulliken spin populations are shown on the schematic structure; populations with absolute values of less than 0.001 are omitted.

alternative yielded enthalpies that were 82 kJ mol^{-1} higher than the selenyl radical species, which is well outside the range of any significant thermal population, indicating that such tautomers are probably unimportant. In Cys–Se•, the spin densities on the two protons of the β -carbons differ, and are lower by an order of magnitude than for the analogous sulfur-based radical previously investigated. Like the thiyl species, the proton oriented closer to the node of the spin density on selenium has a smaller density than that further from the node, suggesting that distinct proton hyperfine couplings for these protons would be observed in electron nuclear double resonance experiments of Cys–Se• or related species.

3.3. Computed Spectra of the Selenyl Radical. Figure 4 compares the DFT StoBe-deMon computed spectra for Cys–Se• and Cys–SeH together with the experimental spectra generated by difference. StoBe-deMon calculations predict an isolated low-energy peak in the XAS of Cys–Se•, in strong support of our conclusion that we have observed X-ray photochemically generated selenyl radical species, and the overall match of computed and experimental spectra is excellent. In addition, the computed spectrum of the selenol Cys–SeH also agrees very well with experiment (Figure 4). As expected, the low-lying transition for Cys–Se• involves the singly occupied molecular orbital. Additionally, the next highest transition at $\sim 12\,261 \text{ eV}$ can be assigned to a $\text{Se}(1s) \rightarrow (\text{Se–C})\sigma^*$ transition, while the $12\,261 \text{ eV}$ peak in the selenol corresponds to close-lying $\text{Se}(1s) \rightarrow (\text{Se–C})\sigma^*$ and $\text{Se}(1s) \rightarrow (\text{Se–H})\sigma^*$ transitions.

3.4. Electron Paramagnetic Resonance (EPR) Spectroscopy. EPR spectroscopy is often considered the method of choice for the study of free radical species. Previous work has discussed the difficulties with observing features of the analogous sulfur-based thiyl radical,^{13,14,36} due to substantial spin–orbit coupling to filled sulfur-based orbitals, with a very broad g_{zz} at the high value of 2.3. With the selenium-based selenyl radical, this broadening and shift to high g -values will be even more pronounced, so that reports of EPR spectra of

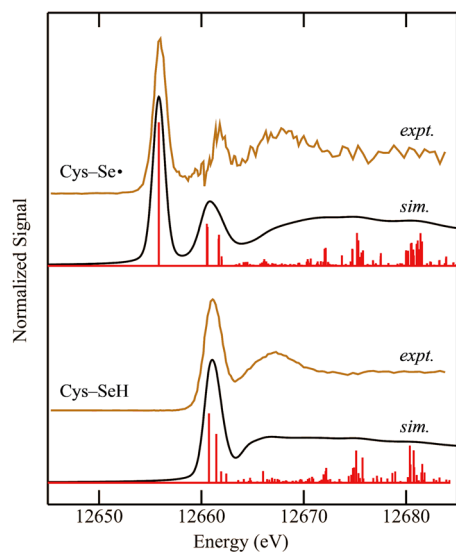


Figure 4. Comparison of the computed HERFD-XAS spectra (*sim.*, black line) with the experimental difference spectra (*expt.*; gold line) for both Cys–Se• and Cys–SeH. The stick spectra of StoBe–DeMon computed transitions are also shown (vertical red lines).

putative selenyl radicals with substantially lower g_{zz} than thyl³⁷ probably arise from other species. Thus, while there are reports of selenium-based free radical systems,³⁸ to date, there have been no authenticated reports of selenyl radical EPR spectra. Figure 5 shows the EPR spectrum of an X-ray irradiated

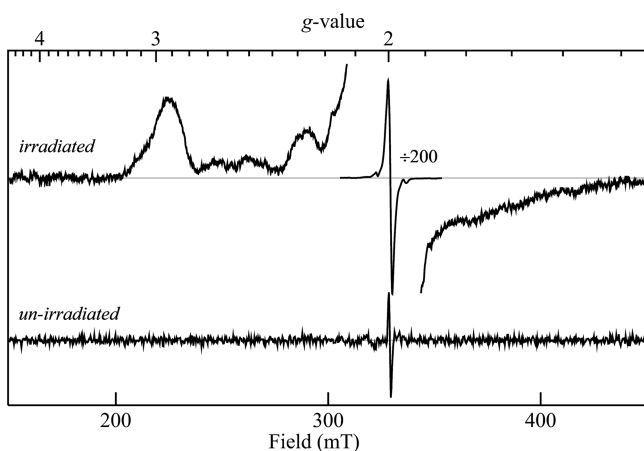


Figure 5. Electron paramagnetic resonance spectra of a sample of selenocysteine prior to (lower trace) and following (upper trace) X-ray irradiation. The gray lines show zero for the different spectra. Spectra were recorded at 80 K using 0.5 mT modulation amplitude with a microwave frequency of 9.194 GHz. The vertical scale of the $g \sim 2.0$ region of the irradiated spectrum has been scaled down by a factor of 200 relative to both the outer spectrum and the un-irradiated spectrum.

aqueous selenocysteine sample. As expected, the spectrum is dominated by an intense $g \sim 2.0$ signal arising from abundant free radical species that are either trapped in the ice matrix or contained in the polyacetal sample cuvette.¹⁶ The EPR signals of selenyl are predicted to occur at either side of the $g \sim 2.0$ signal; since a broad g_{zz} at low field (high g -value) is expected, Figure 5 shows a vertically expanded spectrum. The low signal amplitude is not correlated with an overall low integrated intensity and arises because of the broad nature of the signal

outside the $g \sim 2.0$ region. Examination of the EPR of selenocysteine-containing samples prior to irradiation (Figure 5), and of control samples containing no selenocysteine, showed essentially baseline spectra with no EPR signals apart from the expected $g \sim 2.0$ signal in the irradiated selenocysteine-free sample. The un-irradiated sample did contain a small $g \sim 2.0$ signal (Figure 5); since this signal was also present in the polyacetal cuvette (not illustrated), we conclude that the un-irradiated sample itself is EPR silent. The EPR spectrum of selenyl is expected to be highly anisotropic from spin–orbit coupling with filled selenium-based p-orbitals, and we assign the feature at $g \sim 2.9$ as g_{zz} from this species, with g_{xx} and g_{yy} being expected closer to $g \sim 2.0$. Naturally abundant selenium has a single magnetic isotope ⁷⁷Se at 7.6% abundance with a nuclear spin $I = 1/2$ and a nuclear g -value of 1.074. A sizable ⁷⁷Se hyperfine coupling is expected from the near-unity spin population on selenium, and we therefore expect a sizable and anisotropic ⁷⁷Se hyperfine coupling. While quantitative measurement of this must await experiments using selenocysteine enriched with ⁷⁷Se, it seems probable that some of the structure in Figure 5 may be due to ⁷⁷Se hyperfine. The EPR signal reported here was stable for a period of hours at 100 K and below, indicating that selenyl is a stable commodity in solution at these temperatures.

The present study comprises the first example of the direct detection and characterization of isolated selenium-based free radicals using X-ray absorption spectroscopy, and the first X-ray spectroscopic observation of a selenyl radical. While selenyl radicals may well have been generated with previous XAS experiments,¹⁸ the core-hole broadening of conventional XAS spectra means that such species might be difficult to resolve. Figure 6 shows a comparison of conventional XAS with

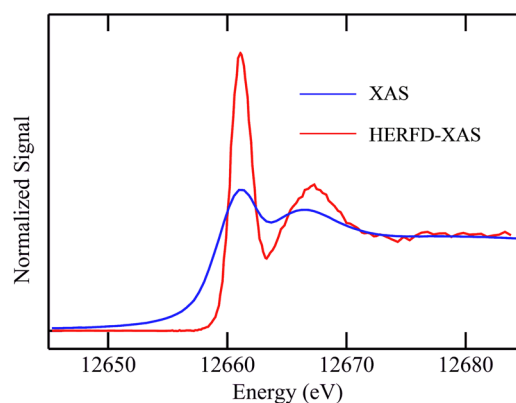


Figure 6. Comparison of XAS with HERFD-XAS for selenocysteine. The XAS spectrum¹⁸ is shown as blue line and the HERFD-XAS by the red line (spectrum of Figure 2). The dramatic improvement in resolution arising from the HERFD-XAS method is clearly apparent.

HERFD-XAS, clearly showing the substantially enhanced resolution of HERFD-XAS measurements. Thus, these observations of the selenyl radical are enabled by high photon flux intensity coupled with the exquisitely high spectral resolution afforded by HERFD-XAS.

The characteristic spectrum of selenyl, with a pronounced low-energy peak arising from the paramagnetic singly occupied molecular orbital, shows some parallels with the well-studied ligand K-edge spectroscopy of transition metal species.^{39,40} These were first understood more than three decades ago, by Sigiura et al.⁴¹ and subsequently by others^{42–46} as due to

covalency between ligand and metal d-orbitals giving partial holes in ligand-based orbitals, resulting in intense dipole-allowed transitions at lower energy than other spectral features. This observation has been exploited extensively for a variety of different chemical and biochemical systems as a direct probe of ligand covalency.^{39,40} To date, such ligand K-edge features have not been reported upon in detail for selenium coordination, but the analogous transitions for sulfur ligands have been very well studied.^{39,40} In general, coordination geometries with more overlap between metal and ligand orbitals tend to have more intense transitions at higher transition energies, whereas those with less overlap tend to have lower intensities, and to be more free-radical-like, arising at lower transition energies. Like the thiyl radical for sulfur,¹³ the selenyl system reported here is expected to represent a low-energy limit below which K-edge associated transitions are not expected to arise.

The reasons behind life's use of selenium in preference to sulfur in some systems are still somewhat unclear.³ First, and as briefly mentioned above, a tremendous metabolic effort is expended by cells in order to incorporate selenium into biological molecules,³ and the process of insertion of selenocysteine is enormously more complex than it is for cysteine or for any of the 19 other canonical amino acids. Second, since selenium itself is also toxic,^{3,4} its use poses an inherent biochemical risk. Selenium enzymes may be favored as they are often much more effective in terms of catalytic rate than their sulfur counterparts. However, another hypothesis as to why selenium is used in preference to sulfur in antioxidant enzymes such as the thioredoxin reductases relates to the inherent differences between the chemistry of thiyl and selenyl radicals. Thus, in these systems, accidental one-electron transfer can generate either thiyl or selenyl radicals with sulfur and selenium enzymes, respectively.¹² The thiyl radical can abstract hydrogen from the protein backbone,⁴⁷ forming carbon centered radicals that could reform thiyl or react with O₂ to form peroxy (O₂·) radicals, resulting in further damage and consequent enzyme inactivation.¹² In contrast, selenyl will not abstract hydrogen, minimizing the risks of inactivation from side-reactions in these systems.¹² Our studies reported here provide both the first direct detection of and a spectroscopic signature for selenyl free radicals, and may provide important tools for directly addressing this chemistry.

AUTHOR INFORMATION

Corresponding Author

*E-mail: g.george@usask.ca.

ORCID

Ingrid J. Pickering: 0000-0002-0936-2994

Graham N. George: 0000-0002-0420-7493

Notes

The authors declare no competing financial interest.

ACKNOWLEDGMENTS

This work was supported by Discovery Grants from the Natural Sciences and Engineering Research Council of Canada (NSERC, I.J.P. and G.N.G.), an Innovation and Science Fund of Saskatchewan grant (I.J.P.), a Canada Foundation for Innovation John Evans Leader's Fund award (I.J.P.) and by Canada Research Chairs (I.J.P. and G.N.G.). S.N. acknowledges funding from the Dr. Rui Feng Scholarship and was a Fellow in the Canadian Institutes of Health Research-Training

grant in Health Research Using Synchrotron Techniques (THRUST). N.V.D. and J.J.H.C. were THRUST Associates. Use of the Stanford Synchrotron Radiation Lightsource, SLAC National Accelerator Laboratory, is supported by the U.S. Department of Energy, Office of Science, Office of Basic Energy Sciences, under Contract No. DE-AC02-76SF00515. The SSRL Structural Molecular Biology Program is supported by the DOE Office of Biological and Environmental Research, and by the National Institutes of Health, National Institute of General Medical Sciences (including P41GM103393). The contents of this publication are solely the responsibility of the authors and do not necessarily represent the official views of NIGMS or NIH.

REFERENCES

- (1) Greenwood, N. N.; Earnshaw, A. *Chemistry of The Elements*, 2nd ed.; Elsevier Butterworth-Heinemann: Jordan Hill, Oxford, U.K., 1996.
- (2) Wedepohl, K. H. The Composition of the Continental Crust. *Geochim. Cosmochim. Acta* **1995**, *59*, 1217–1232.
- (3) Reich, H. J.; Hondal, R. J. Why Nature Chose Selenium. *ACS Chem. Biol.* **2016**, *11*, 821–841.
- (4) Jukes, T. H. Selenium, an "Essential Poison". *J. Appl. Biochem.* **1983**, *5*, 233–234.
- (5) Dénès, F.; Pichowicz, M.; Povie, G.; Renaud, P. Thiyl Radicals in Organic Synthesis. *Chem. Rev.* **2014**, *114*, 2587–2593.
- (6) Trujillo, M.; Alvarez, B.; Radi, R. One- and Two-electron Oxidation of Thiols: Mechanisms, Kinetics and Biological Fates. *Free Radical Res.* **2016**, *50*, 150–171.
- (7) Schöneich, C. Thiyl Radicals and Induction of Protein Degradation. *Free Radical Res.* **2016**, *50*, 143–149.
- (8) Stoyanovsky, D.; Maeda, A.; Atkins, J. L.; Kagan, V. E. Assessments of Thiyl Radicals in Biosystems: Difficulties and New Applications. *Anal. Chem.* **2011**, *83*, 6432–6438.
- (9) Minnihan, E. C.; Nocera, D. G.; Stubbe, J. Long-Range Radical Transfer in *E. coli* Class Ia Ribonucleotide Reductase. *Acc. Chem. Res.* **2013**, *46*, 2524–2535.
- (10) Deryagina, E. N.; Voronkov, M. G.; Korchevin, N. A. Selenium- and Tellurium-centered Radicals. *Russ. Chem. Rev.* **1993**, *62*, 1107–1117.
- (11) Mishra, B.; Kumbhare, L. B.; Jain, V. K.; Priyadarsini, K. I. Pulse Radiolysis Studies on Reactions of Hydroxyl Radicals with Selenocysteine Derivatives. *J. Phys. Chem. B* **2008**, *112*, 4441–4446.
- (12) Nauser, T.; Steinmann, D.; Grassi, G.; Koppenol, W. H. Why Selenocysteine Replaces Cysteine in Thioredoxin Reductase: A Radical Hypothesis. *Biochemistry* **2014**, *53*, 5017–5022.
- (13) Sneed, E. Y.; Hackett, M. J.; Cotelesage, J. J. H.; Prince, R. C.; Barney, M.; Goto, K.; Block, E.; Pickering, I. J.; George, G. N. Photochemically-generated thiyl free radicals observed by X-ray absorption spectroscopy. *J. Am. Chem. Soc.* **2017**, *139*, 11519–11526.
- (14) Martin-Diaconescu, V.; Kennepohl, P. Sulfur K-edge XAS as a Probe of Sulfur-Centered Radical Intermediates. *J. Am. Chem. Soc.* **2007**, *129*, 3034–3035.
- (15) Ochmann, M.; von Ahnen, I.; Cordones, A. A.; Hussain, A.; Lee, J. H.; Hong, K.; Adamczyk, K.; Vendrell, O.; Kim, T. K.; Schoenlein, R. W.; Huse, N. Light-Induced Radical Formation and Isomerization of an Aromatic Thiol in Solution Followed by Time-Resolved X-ray Absorption Spectroscopy at the Sulfur K-Edge. *J. Am. Chem. Soc.* **2017**, *139*, 4797–4804.
- (16) Nienaber, K. H.; Pushie, M. J.; Cotelesage, J. J. H.; Pickering, I. J.; George, G. N. Cryoprotectants Remarkably Exacerbate X-ray Induced Photoreduction. *J. Phys. Chem. Lett.* **2018**, *9*, 540–544.
- (17) George, G. N.; Pickering, I. J.; Pushie, M. J.; Nienaber, K.; Hackett, M. J.; Ascone, I.; Hedman, B.; Hodgson, K. O.; Aitken, J. B.; Levina, A.; Glover, C.; Lay, P. A. X-ray Induced Photo-Chemistry and X-ray Absorption Spectroscopy of Biological Samples. *J. Synchrotron Radiat.* **2012**, *19*, 875–886.

- (18) Pickering, I. J.; George, G. N.; van Fleet-Stalder, V.; Chasteen, T. G.; Prince, R. C. X-ray Absorption Spectroscopy of Selenium-Containing Amino Acids. *JBIC, J. Biol. Inorg. Chem.* **1999**, *4*, 791–794.
- (19) Sokaras, D.; Weng, T.-C.; Nordlund, D.; Alonso-Mori, R.; Velikov, P.; Wenger, D.; Garachtchenko, A.; George, M.; Borzenets, V.; Johnson, B.; Rabedeau, T.; Bergmann, U. A Seven-Crystal Johann-type Hard X-ray Spectrometer at the Stanford Synchrotron Radiation Lightsource. *Rev. Sci. Instrum.* **2013**, *84*, 053102.
- (20) George, G. N.; Garrett, R. M.; Prince, R. C.; Rajagopalan, K. V. The Molybdenum Site of Sulfite Oxidase: A Comparison of Wild-Type and the Cysteine 207 to Serine Mutant using X-ray Absorption Spectroscopy. *J. Am. Chem. Soc.* **1996**, *118*, 8588–8592.
- (21) Delley, B. An All-Electron Numerical Method for Solving the Local Density Functional for Polyatomic Molecules. *J. Chem. Phys.* **1990**, *92*, 508–517.
- (22) Delley, B. From molecules to solids with the DMol³ approach. *J. Chem. Phys.* **2000**, *113*, 7756–7764.
- (23) Perdew, J. P.; Burke, K.; Ernzerhof, M. Generalized Gradient Approximation Made Simple. *Phys. Rev. Lett.* **1996**, *77*, 3865–3868.
- (24) Perdew, J. P.; Burke, K.; Ernzerhof, M. Generalized Gradient Approximation Made Simple. *Phys. Rev. Lett.* **1996**, *77*, 3865–3868; *Phys. Rev. Lett.* **1997**, *78*, 1396.
- (25) Klamt, A.; Schüürmann, G. COSMO: A New Approach to Dielectric Screening in Solvents with Explicit Expressions for the Screening Energy and its Gradient. *J. Chem. Soc., Perkin Trans. 2* **1993**, *2*, 799–805.
- (26) Hermann, K.; Pettersson, L. G. M.; Casida, M. E.; Daul, C.; Goursoot, A.; Koester, A.; Proynov, E.; St-Amant, A.; Salahub, D. R.; Carravetta, V.; Duarte, H.; Godbout, N.; Guan, J.; Jamorski, C.; Leboeuf, M.; Malkin, V.; Malkina, O.; Nyberg, M.; Pedocchi, L.; Sim, F.; Triguero, L.; Vela, A. *StoBe-deMon Code*; 2001.
- (27) Perdew, J. P.; Yue, W. Accurate and Simple Density Functional for the Electronic Exchange Energy: Generalized Gradient Approximation. *Phys. Rev. B: Condens. Matter Mater. Phys.* **1986**, *33*, 8800.
- (28) Perdew, J. P. Density-Functional Approximation for the Correlation Energy of the Inhomogeneous Electron Gas. *Phys. Rev. B: Condens. Matter Mater. Phys.* **1986**, *33*, 8822–8824.
- (29) Perdew, J. P. Erratum: Density-Functional Approximation for the Correlation Energy of the Inhomogeneous Electron Gas. *Phys. Rev. B: Condens. Matter Mater. Phys.* **1986**, *34*, 7406.
- (30) Doonan, C. J.; Rubie, N. D.; Peariso, K.; Harris, H. H.; Knottenbelt, S. Z.; George, G. N.; Young, C. G.; Kirk, M. L. Electronic Structure Description of the cis-MoOS Unit in Models for Molybdenum Hydroxylases. *J. Am. Chem. Soc.* **2008**, *130*, 55–65.
- (31) Hämmäläinen, K.; Siddons, D. P.; Hastings, J. B.; Berman, L. E. Elimination of the Inner-Shell Lifetime Broadening in X-ray-Absorption Spectroscopy. *Phys. Rev. Lett.* **1991**, *67*, 2850–2853.
- (32) de Groot, F. M. F.; Krisch, M. H.; Vogel, J. Spectral Sharpening of the Pt L Edges by High-Resolution X-ray Emission. *Phys. Rev. B: Condens. Matter Mater. Phys.* **2002**, *66*, 195112.
- (33) Byun, B. J.; Kang, Y. K. Conformational Preferences and pKa Value of Selenocysteine Residue. *Biopolymers* **2011**, *95*, 345–353.
- (34) Mesu, J. G.; Beale, A. M.; de Groot, F. M.; Weckhuysen, B. M. Probing the Influence of X-rays on Aqueous Copper Solutions Using Time-Resolved in Situ Combined Video/X-ray Absorption Near-Edge/Ultraviolet-Visible Spectroscopy. *J. Phys. Chem. B* **2006**, *110*, 17671–17677.
- (35) Leeck, D. T.; Li, R.; Chyall, L. J.; Kenttämaa, H. I. Homolytic Se-H Bond Energy and Ionization Energy of Benzeneselenol and the Acidity of the Corresponding Radical Cation. *J. Phys. Chem.* **1996**, *100*, 6608–6611.
- (36) Lassmann, G.; Kolberg, M.; Bleifuss, G.; Gräslund, A.; Sjöberg, B.-M.; Lubitz, W. *Phys. Chem. Chem. Phys.* **2003**, *5*, 2442–2453.
- (37) Windle, J. J.; Wiersema, A. K.; Tappel, A. L. Electron Paramagnetic Resonance of Some Sulfur and Selenium Compounds. *J. Chem. Phys.* **1964**, *41*, 1996–2002.
- (38) Mallow, O.; Khanfar, M. O.; Malischewski, M.; Finke, P.; Hesse, M.; Lork, E.; Augenstein, T.; Breher, F.; Harmer, J. R.; Vasilieva, N. V.; Zibarev, A.; Bogomyakov, A. S.; Seppelt, K.; Beckmann, J. Diaryldichalcogenide Radical Cations. *Chem. Sci.* **2015**, *6*, 497–504.
- (39) Glaser, T.; Hedman, B.; Hodgson, K. O.; Solomon, E. I. Ligand K-edge X-ray Absorption Spectroscopy: A Direct Probe of Ligand–Metal Covalency. *Acc. Chem. Res.* **2000**, *33*, 859–868.
- (40) Solomon, E. I.; Hedman, B.; Hodgson, K. O.; Dey, A.; Szilagy, R. K. Ligand K-edge Spectroscopy Covalency of Ligand–Metal Bonds. *Coord. Chem. Rev.* **2005**, *249*, 97–129.
- (41) Sugiura, C.; Kitamura, M.; Muramatsu, S. X-ray Absorption Near-Edge Structure of Complex Compounds (NH₄)₃RhCl₆, K₃RuCl₆, and Ru(NH₃)₆Cl₃. *J. Chem. Phys.* **1986**, *84*, 4824–4827.
- (42) Nakai, S.; Kawata, A.; Ohashi, M.; Kitamura, M.; Sugiura, C.; Mitsuishi, T.; Maezawa, H. Core-exciton Absorption in the F K Absorption Spectra of 3d Transition-Metal Fluorides. *Phys. Rev. B: Condens. Matter Mater. Phys.* **1988**, *37*, 10895–10897.
- (43) de Groot, F. M. F.; Grioni, M.; Fuggle, J. C.; Ghijsen, J.; Sawatzky, G. A.; Petersen, H. Oxygen 1s X-ray-Absorption Edges of Transition-Metal Oxides. *Phys. Rev. B: Condens. Matter Mater. Phys.* **1989**, *40*, 5715–5723.
- (44) Hedman, B.; Hodgson, K. O.; Solomon, E. I. X-ray Absorption Edge Spectroscopy of Ligands Bound to Open-Shell Metal Ions: Chlorine K-edge Studies of Covalency in Tetrachlorocuprate(2-). *J. Am. Chem. Soc.* **1990**, *112*, 1643–1645.
- (45) Shadle, S. E.; Hedman, B.; Hodgson, K. O.; Solomon, E. I. Ligand K-edge X-ray Absorption Spectroscopic Studies: Metal-Ligand Covalency in a Series of Transition Metal Tetrachlorides. *J. Am. Chem. Soc.* **1995**, *117*, 2259–2272.
- (46) Pickering, I. J.; George, G. N. Polarized X-ray Absorption Spectroscopy of Cupric Chloride Dihydrate. *Inorg. Chem.* **1995**, *34*, 3142–3152.
- (47) Nauser, T.; Schöneich, C. Thiyl Radicals Abstract Hydrogen Atoms from the α -C–H Bonds in Model Peptides: Absolute Rate Constants and Effect of Amino Acid Structures. *J. Am. Chem. Soc.* **2003**, *125*, 2042–2043.